European Journal of Medicinal Chemistry 220 (2021) 113484

Contents lists available at ScienceDirect

European Journal of Medicinal Chemistry

journal homepage: http://www.elsevier.com/locate/ejmech

Structure-based bioisosterism design of thio-benzoxazepinones as novel necroptosis inhibitors

Chunnian Xia [a, 1], Zhengguang Yao [a, b, 1], Lijuan Xu [b, c], Wannian Zhang [b, c], Haihu Chen [d, **], Chunlin Zhuang [b, c, *]

[a] School of Pharmacy, Zhejiang University of Technology, Hangzhou, 310014, China
[b] School of Pharmacy, Second Military Medical University, 325 Guohe Road, Shanghai, 200433, China
[c] School of Pharmacy, Ningxia Medical University, Yinchuan, 750004, China
[d] Department of Intervention, Changhai Hospital, Second Military Medical University, Shanghai, 200433, China

ARTICLE INFO

Article history:
Received 25 January 2021
Received in revised form
2 April 2021
Accepted 15 April 2021
Available online 27 April 2021

Keywords:
Bioisosterism
Thio-benzoxazepinone
Necroptosis
Chirality

ABSTRACT

Necroptosis is reported to play a critical role in contributing to a variety of human pathologies. The benzoxazepinone GSK′772 is a potent necroptosis inhibitor optimized using a hit from a DNA-encoded library, which is currently in phase II clinical trials for psoriasis, rheumatoid arthritis, and ulcerative colitis. In the present study, the bioisosterism strategy was applied to replace the amide and benzene ring of GSK′772 based on the co-crystal structure of GSK′772 with its binding target RIPK1. As a result, the novel thio-benzoxazepinones exhibited higher anti-necroptosis activity in a human HT-29 cell necroptosis model. The effect on anti-necroptosis activity by the chirality was significantly reduced in the thio-benzoxazepinones, which was explained by the ligand conformation calculation. Among these analogues, compound **11** (S) and **12** (R) specifically inhibited necroptosis rather than apoptosis with EC_{50} values of 2.8 and 22.6 nM. They blocked necrosome formation by inhibiting the phosphorylation of RIPK1, RIPK3 and MLKL in necroptotic cells. Collectively, the highly potent thio-benzoxazepinones represent promising lead structures for further development of necroptosis-related diseases.

1. Introduction

Necroptosis is gradually characterized as a new form of programmed cell death (PCD) that occurs at conditions of blocking the execution of apoptosis [1,2]. It has been reported to be associated with various lethal inflammation and pathology [3]. Targeting the pathologic necroptosis pathway has been recognized as a very important strategy for the inflammatory diseases [4,5]. With the identification of necrostatins as the first series of necroptosis inhibitors, the binding target, receptor-interacting protein kinase 1 (RIPK1), has emerged as a critical driver of TNF-mediated necroptosis [6,7]. Then, RIPK1 interacts with the RIP homotypic interaction motif (RHIM) on the downstream RIPK3, together initiating the formation of necrosomes and activating RIPK3 via phosphorylation [8,9]. Subsequently, phosphorylation of RIPK3 results in the recruitment and phosphorylation of mixed lineage kinase domain-like protein (MLKL) [10,11]. With the phosphorylated MLKL, oligomerizes are formed and translocated into the plasma membrane to trigger membrane rupture, initiating necroptosis [10,12–14]. Thus, targeting the upstream RIPK1 has been shown to have broad

Abbreviations: DEL, DNA-encoded library; DIPEA, *N,N*-Diisopropylethylamine; DMEM, Dulbecco's modified Eagle's medium; FBS, fetal bovine serum; HATU, 2-(7-Azabenzotriazol-1-yl)-N,N,N′,N′-tetramethyluronium hexafluorophosphate; HPLC, high-performance liquid chromatography; hTNF-α, human tumor necrosis factor-a; MLKL, mixed lineage kinase domain-like protein; PBS, phosphate buffer saline; PCD, programmed cell death; PDAC, pancreatic ductal adenocarcinoma cancer; RHIM, RIP homotypic interaction motif; RIPK1, receptor-interacting protein kinase 1; RIPK3, receptor-interacting protein kinase 3; SDS-PAGE, sodium dodecyl sulfate-polyacrylamide gel electrophoresis; TNF-α, tumor necrosis factor-α; TLC, thin layer chromatography; TS, TNF-α, Smac mimetic; TSZ, TNF-α, Smac mimetic and z-VAD-fmk; TTC, 2,3,5-triphenyl tetrazolium chloride.

* Corresponding author. School of Pharmacy, Second Military Medical University, 325 Guohe Road, Shanghai, 200433, China.
** Corresponding author.
E-mail addresses: chenhaihu666@foxmail.com (H. Chen), zclnathan@163.com (C. Zhuang).
[1] These authors contributed equally to this work.

https://doi.org/10.1016/j.ejmech.2021.113484
0223-5234/

therapeutic potentials for multiple necroptosis-related diseases.

From 2005 to the present, more than 20 classes of necroptosis inhibitors have been published [15]. GlaxoSmithKline (GSK) has made great contributions in the discovery of necroptosis inhibitors (Fig. 1). From a prioritized DNA-encoded library (DEL), the benzo[b][1,4]xazepin-4-one scaffold was found to be potent as a necroptosis inhibitor, which was then optimized to yield benzoxazepinone GSK′481 (U937 cell, IC_{50} = 10 nM) [16]. This compound had an extremely high RIPK1 target specificity, exhibiting a >7500-fold selectivity window at a concentration of 10 μM against other 400 kinases. Further optimizations of GSK′481 for improving the drug properties obtained GSK′772, possessing highly RIPK1 selective inhibitory activity. This compound has been advanced into phase II trials in several inflammatory indications (ulcerative colitis, NCT02903966; psoriasis, NCT02776033; rheumatoid arthritis, NCT02858492) [16–19]. Another fluoro-containing analogue GSK′095 is progressed to phase I/II trials in subjects with pancreatic ductal adenocarcinoma cancer (PDAC) and other tumors (NCT03681951) [20].

In the present study, we applied GSK′772 as the lead compound, with the purpose to generate derivatives by bioisosterism design to explore new inhibitors for necroptosis. Another aim of this study is to determine the importance of the chirality in the different benzoxazepinone fragments on the anti-necroptosis activity.

2. Results and DISCUSSION

2.1. Design rationale

The reported X-ray co-crystal structure of RIPK1 binding with GSK′772 (PDB code: 5TX5, Fig. 2A) [18] showed that GSK′772 occupied the allosteric lipophilic pocket at the back of the ATP binding site and no interactions with the hinge residues of the RIPK1 kinase. The amide carbonyl group formed a hydrogen-bonding interaction with the backbone amide NH of D156, playing a critical role in the anti-necroptosis activity. Besides, a water-mediated hydrogen-bonding interaction was observed between the triazole and M67. However, the carbonyl group of the benzoxazepinone fragment did not show any hydrogen-bonding interaction with surrounding residues, indicating as a potential modifiable site. Thus, the benzene ring was substituted or changed by heterocycles via a bioisosterism strategy as it did not attach with the hinge region (Fig. 2B). Similarly, we also attempted to replace the carbonyl by a thiocarbonyl group in order to provide new lead compounds as necroptosis inhibitors following our previous studies [21,22]. In addition, the chirality of the molecules with thiocarbonyl groups affecting the activity were also determined.

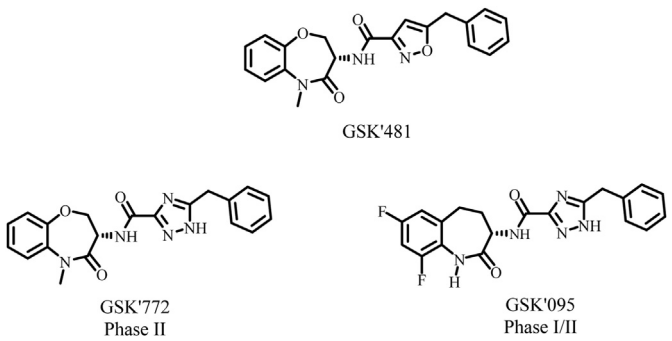

Fig. 1. The chemical structures of GSK′481, GSK′772 and GSK′095 in the clinical development.

2.2. Chemistry

The benzoxazepinones were synthesized following the GSK reported procedure as outlined in Scheme 1 [16,18]. Briefly, the key intermediates **m5** were generated from the commercial 1-fluoro-2-nitro-benzene/heterocycles and Boc-L-serine or Boc-D-serine by a nucleophilic aromatic substitution, reduction, cyclization and alkylation reactions. Treatment of **m5** with the Lawesson's reagent afforded thio-benzoxazepinones **m6**. Finally, de-protecting the Boc group with HCl and reaction with 5-benzyl-1H-1,2,4-triazole-3-carboxylic acid [23] under amide coupling conditions provided target compounds **1**–**26**. The final structures were fully characterized by ^{1}H NMR, ^{13}C NMR, and HRMS. All target compounds were purified to >95%, as determined by high-performance liquid chromatography (HPLC) analysis, prior to use in subsequent experiments.

2.3. Biological evaluation and SAR study

First, we tried to confirm the anti-necroptosis activity of the benzoxazepinones with different chirality, which has not been fully characterized in the previous publications [16,18]. As shown in Table 1, the benzene ring was changed by different pyridinyl groups, and the two conformations using D- and L-serine were obtained. Consistent with GSK reports [18,20], compound **1** (GSK′772, S-configuration) exhibited an EC_{50} value of 0.0036 μM and compound **2** with R-configuration was only 78-fold lower (EC_{50} = 0.2792 μM) in the HT-29 necroptosis cell model. The Nec-1s was applied as a positive control with an EC_{50} of 0.2112 μM. When the benzene ring was replaced by different pyridines, a same trend but lower activity than the benzene analogues was observed. Compounds **3** and **4** showed no apparent activity at 10 μM. With one more methyl group on the pyridine ring, compounds **5** and **7** with S-configurations improved the activity (EC_{50} = 0.3630, 0.2430 μM). The corresponding compounds **6** and **8** with R-configurations showed much lower activity. When the pyridine ring was flipped, the anti-necroptosis activity of compounds **9** and **10** were significantly improved. These compounds did not show apparent cytotoxicity at 50 μM.

Next, the thio-benzoxazepinones were evaluated (Table 2). Overall, these compounds with the S configurations maintained the potent anti-necroptosis activity, and especially, the analogues with the R configurations significantly improved the activity. The activity was about 10-fold lower than those of S-analogues (>70-fold in benzoxazepinones), indicating the reduced influence on the activity by the chiral center. Compound **11** (S-configuration) showed an EC_{50} value of 0.0028 μM, while compound **12** (R-configuration) had an EC_{50} of 0.0226 μM. Compounds **13** and **14** without the *N*-methyl group showed dramatically decreased activity (EC_{50} = 0.7356, 8.8370 μM), highlighting the importance of the *N*-alkylation. The deuterated methyl substituted compounds **15** and **16** showed comparable potency as the corresponding methyl analogues **11**–**12**. However, the ethylated compounds **17** and **18** made the activity sharply decreased (EC_{50} = 1.5130, 6.6770 μM). This result was consistent with the co-crystal complex where the *N*-methyl group of GSK′772 was located at the small subpocket of L90 and I43 residues (Fig. 1), indicating the insufficient chemical space for the ethyl group. Consequently, the benzene ring was also replaced by pyridines (**19**–**24**). Consistent with the pyridine-xazepinones in Table 1, these compounds showed much lower activity than the thio-benzoxazepinone analogues. Compounds **25** and **26** with the pyridine flipped, exhibited the anti-necroptosis activity improved with EC_{50} values of 0.0137 and 0.0186 μM. At 50 μM, these thio-benzoxazepinone compounds did not show any apparent cytotoxicity.

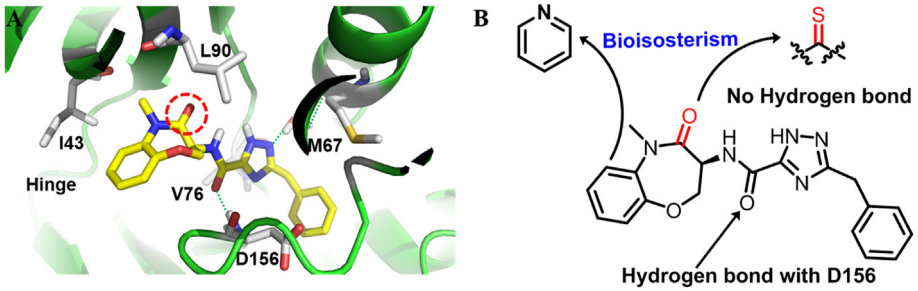

Fig. 2. (A) Co-crystal binding structure of RIPK1 with GSK′772 (PDB code: 5TX5) and (B) the bioisosterism strategy of the new thio-benzoxazepinones.

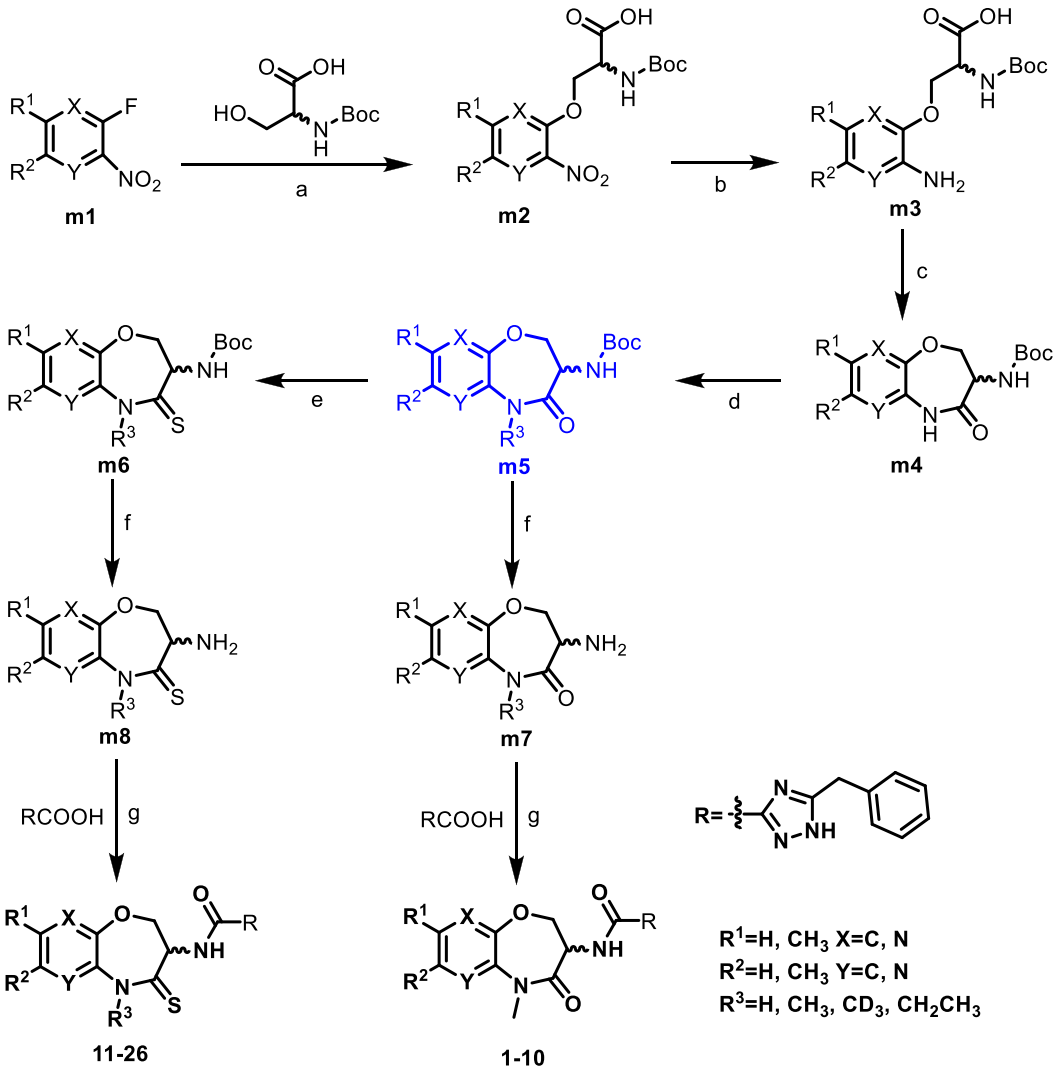

Scheme 1. Synthetic route of the benzoxazepinones and thio-benzoxazepinones. Reagents and conditions: (a) NaH, DMF, room temperature, 40–77%; (b) H_2, Pd/C, MeOH, room temperature, 80–98%; (c) HATU, DIPEA, DMSO, room temperature, 30–50%; (d) R^3I, Cs_2CO_3, DMF, room temperature, 40–70%; (e) Lawesson's reagent, toluene, 115 °C, 30–60%. (f) HCl, DCM, room temperature, 50–90%; (g) HATU, DIPEA, DMSO, room temperature, 70–90%.

2.4. Ligand-based explanation on the activity of different configurations

Based on the above biological results, the chiral benzoxazepinones and thio-benzoxazepinones showed quite different configuration activity properties. In order to predict the configuration profiles, the three-dimensional conformations of representative compounds were calculated by the Schrodinger ligand conformation calculation. As illustrated in Fig. 3, GSK′772 with S-configuration (yellow) and compound **2** with R-configuration (green) possessed different forms, probably making a large difference in anti-necroptosis activity (>70-fold). It is known that the C=S with higher bond length than C=O might result in improved steric hindrance. The C=O containing compound is more

Table 1
The chemical structures of benzoxazepinones and the anti-necroptosis activity.

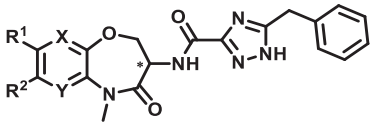

Compound	X	Y	R^1	R^2	Configuration (S/R)	Antinecroptosis (EC_{50}, μM)[a]	Cytotoxicity (CC_{50}, μM)
1 (GSK'772)	C	C	H	H	S	0.0036 ± 0.0001	>50
2	C	C	H	H	R	0.2792 ± 0.00537	>50
3	N	C	H	H	S	>10	>50
4	N	C	H	H	R	>10	>50
5	N	C	CH_3	H	S	0.3630 ± 0.0281	>50
6	N	C	CH_3	H	R	6.4960	>50
7	N	C	H	CH_3	S	0.2430 ± 0.0142	>50
8	N	C	H	CH_3	R	>10	>50
9	C	N	H	H	S	0.0154 ± 0.0037	>50
10	C	N	H	H	R	0.8105 ± 0.0477	>50
Nec-1s	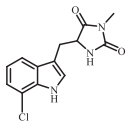				/	0.2112 ± 0.0071	>50

[a] Human HT-29 cells were pretreated with DMSO or the test compound and then stimulated with hTNF-α (20 ng/mL), Smac mimetic (10 nM), and z-VAD-fmk (20 μM) (TSZ) for 8–10 h. The inhibition of TSZ-induced necroptosis in HT-29 cells is presented as the EC_{50} ± SD. The SD value was not determined if the EC_{50} > 1 μM. All experiments were repeated independently at least 3 times.

Table 2
The chemical structures of thio-benzoxazepinones and the anti-necroptosis activity.

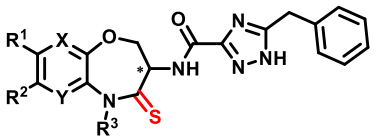

Compound	X	Y	R^1	R^2	R^3	Configuration (S/R)	Antinecroptosis (EC_{50}, μM)[a]	Cytotoxicity (CC_{50}, μM)
11	C	C	H	H	CH_3	S	0.0028 ± 0.0002	>50
12	C	C	H	H	CH_3	R	0.0226 ± 0.0034	>50
13	C	C	H	H	H	S	0.7356 ± 0.0428	>50
14	C	C	H	H	H	R	8.8370	>50
15	C	C	H	H	CD_3	S	0.0074 ± 0.0011	>50
16	C	C	H	H	CD_3	R	0.0763 ± 0.0042	>50
17	C	C	H	H	CH_2CH_3	S	1.5130	>50
18	C	C	H	H	CH_2CH_3	R	6.6770	>50
19	N	C	H	H	CH_3	S	>10	>50
20	N	C	H	H	CH_3	R	>10	>50
21	N	C	CH_3	H	CH_3	S	0.1218 ± 0.0141	>50
22	N	C	CH_3	H	CH_3	R	2.0175	>50
23	N	C	H	CH_3	CH_3	S	0.1438 ± 0.0260	>50
24	N	C	H	CH_3	CH_3	R	3.4025	>50
25	C	N	H	H	CH_3	S	0.0137 ± 0.0038	>50
26	C	N	H	H	CH_3	R	0.0186 ± 0.0003	>50

[a] Human HT-29 cells were pretreated with DMSO or the test compound and then stimulated with hTNF-α (20 ng/mL), Smac mimetic (10 nM), and z-VAD-fmk (20 μM) (TSZ) for 8–10 h. The inhibition of TSZ-induced necroptosis in HT-29 cells is presented as the EC_{50} ± SD. The SD value was not determined if the EC_{50} > 1 μM. All experiments were repeated independently at least 3 times.

flexible with a higher bond angle than the more restricted C=S compound. Thus, the thio-benzoxazepinone compound **11** (S, yellow) and compound **12** (R, green) showed similar conformations, probably leading to their small differences in activity.

2.5. Compounds 11 and 12 specifically inhibit necroptosis not apoptosis

As the thio-benzoxazepinone compounds **11** and **12** showed the best activity in this series, we next selected them to evaluate their antinecroptotic abilities in cells. The starting concentration for compound **12** was set 10-fold higher than that of **11** and gradually decreased according to their EC_{50} values. As shown in Fig. 4A and B, they efficiently restored cell viability from TSZ-induced necroptosis in a dose-response manner. And they did not protected cells from TS-induced apoptosis (Fig. 4C and D), indicating that these compounds specifically inhibited the necroptosis.

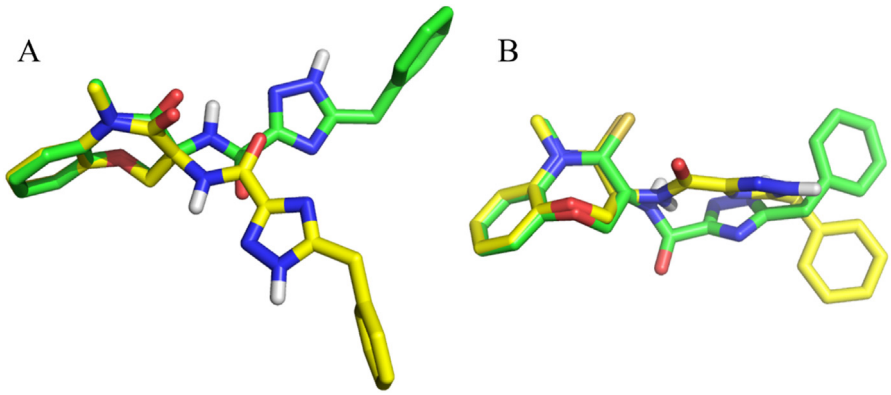

Fig. 3. Structure predictions for different configurations. (A) GSK′772 (S, yellow) and compound **2** (R, green); (B) Thio-benzoxazepinone compound **11** (S, yellow) and compound **12** (R, green).

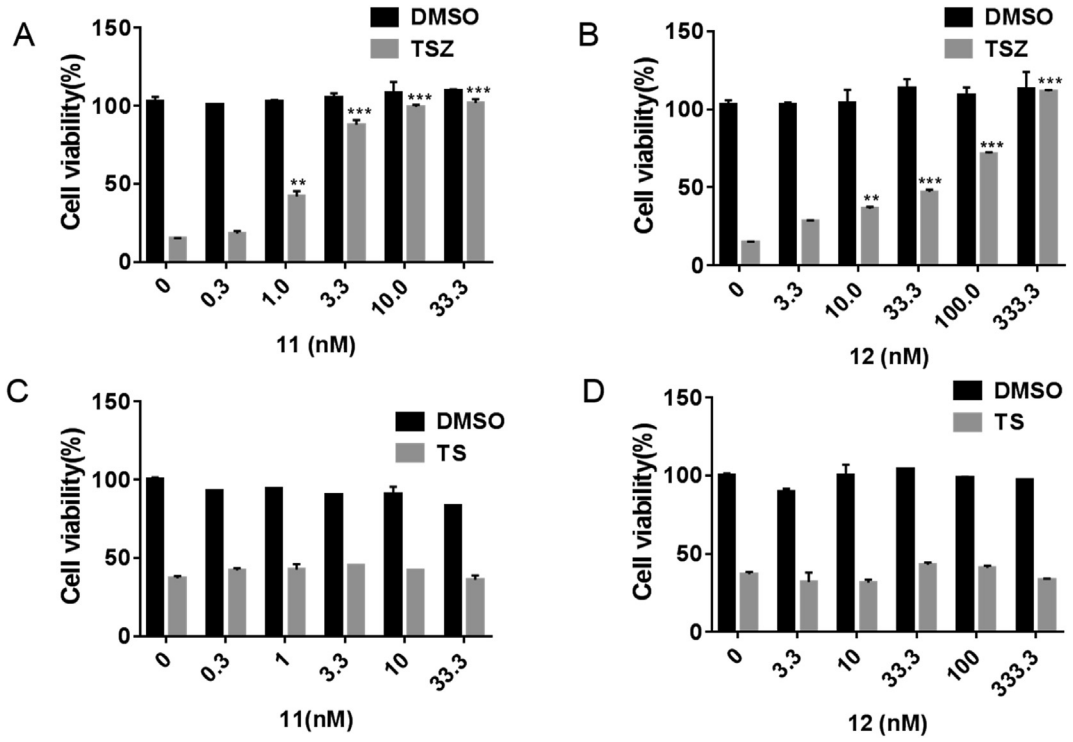

Fig. 4. Effects of compounds 11 and 12 on necroptosis in vitro. HT-29 cells were treated compound **11** (A) and compound **12** (B) as indicated concentrations followed by stimulation with TSZ for 8−10 h. HT-29 cells were treated with various concentrations of compound **11** (C) and compound **12** (D) as indicated by stimulation with TS for 30 h (*p < 0.05, **p < 0.01, ***p < 0.001 versus TSZ, TS simulation without compound treatment).

2.6. Compounds 11 and 12 blocks necrosome formation by inhibiting the phosphorylation of RIPK1 and RIPK3

Then, we examined phosphorylation of RIPK1, RIPK3, and MLKL in TSZ-treated HT-29 cell model with or without compounds **11** and **12** in order to investigate their inhibitory mechanism against necroptosis. Considering the benzoxazepinones were confirmed as RIPK1 selective inhibitors, it should regulate the downstream RIPK3 and MLKL.[9] Consistently, the thio-benzoxazepinones **11** and **12** completely inhibited the phosphorylation of both RIPK1 and RIPK3 at 1 μM, and subsequently inhibited the downstream phosphorylation of MLKL (Fig. 5A). As shown in Fig. 5B, compounds **11** and **12** inhibited the phosphorylation of RIPK1/3 and MLKL at 4 h in a dose-response manner (0.001, 0.01, 0.1 and 1 μM). As the phosphorylation of RIPK1 and RIPK3 is essential for RIPK1-RIPK3 necrosome formation,[8] we then examined the necrosome formation in thio-benzoxazepinones-treated HT-29 cells. We found that they completely blocked TSZ-induced necrosome formation at 1 μM for inhibiting the necroptosis (Fig. 5C).

3. Conclusion

With the purpose to develop new analogues based on the phase II clinical candidate GSK′772, the bioisosterism strategy was applied in the present study. Novel thio-benzoxazepinones were developed, maintaining the high anti-necroptosis activity in human HT-29 cell necroptosis model for the S-configuration. The anti-necroptosis activity for the R-configuration was improved significantly compared with the corresponding R-benzoxazepinones. The configuration profiles of these chiral compounds were analyzed by

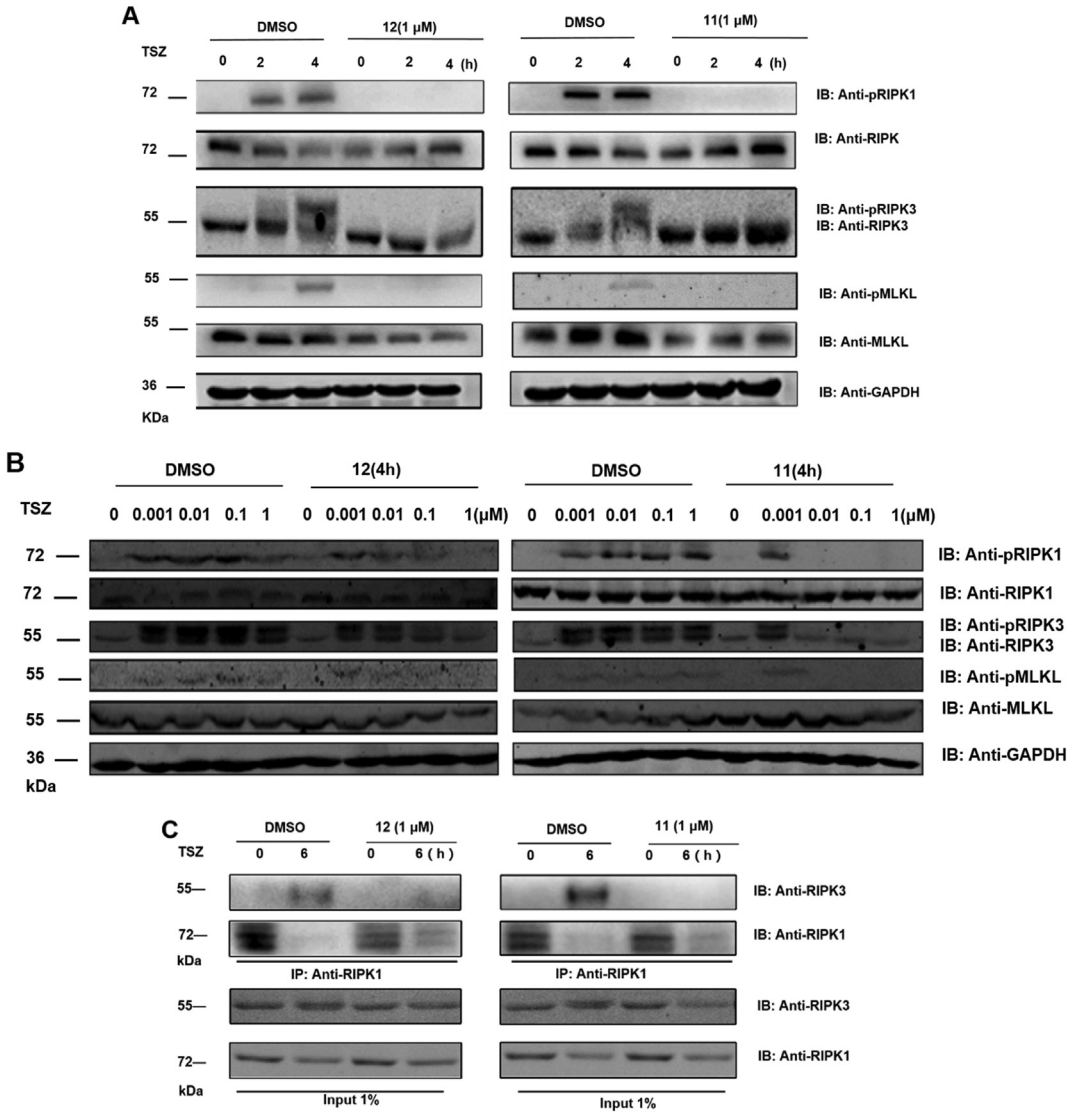

Fig. 5. Compounds 11 and 12 block necrosome formation by inhibiting the RIPK1/RIPK3/MLKL pathway. (A) HT-29 cells were pretreated with compound (1 μM) followed by stimulation with TSZ at the indicated time points. Cells were lysed and immunoblotted with the indicated antibodies. (B) HT-29 cells were pretreated with compound (0, 0.001, 0.01, 0.1, 1 μM) and then stimulated with TSZ for 4 h. Cells were lysed and immunoblotted with the indicated antibodies. (C) HT-29 cells were treated with DMSO or compound (1 μM) for 6 h. The cell lysates were immunoprecipitated with an anti-RIPK1 antibody (IP: RIPK1) and analyzed by immunoblotting with the indicated antibodies.

Schrodinger ligand conformation calculation. Our results suggested that the thio-benzoxazepinones could be lead compounds for discovering more inhibitors for further development of necroptosis-related diseases.

4. Experimental section

4.1. Chemistry

All starting materials were obtained from commercial sources and were analytically pure. The ^{1}H NMR and ^{13}C NMR spectra were recorded on Bruker Avance 300 and 600 MHz spectrometers (Bruker Company, Germany) using tetramethylsilane as an internal standard and $CDCl_3$ or DMSO-d_6 as solvents. Chemical shifts (δ values) and coupling constants (J values) are given in ppm and hertz (Hz), respectively. High-resolution mass spectrometry data were acquired using a quadrupole time-of-flight micro mass spectrometer. Thin-layer chromatography (TLC) analyses were carried out on silica gel plates GF254 (Qingdao Haiyang Chemical, China). Column chromatography separations were carried out on a silica gel 200–300 mesh. The purities of the compounds were analyzed by HPLC (Agilent 1260) using a C18 column (Elite Hypersil ODS2, 4.6 × 250 mm, 5 μm) with 85% methanol/15% water as the mobile phase at a flow rate of 2 mL/min, and all final compounds exhibited purities greater than 95%.

4.2. General procedure for the preparation of compounds ***1*–*26***

To a solution of *N*-Boc-serine (1 equiv) in DMF was added dropwise to a suspension of sodium hydride (2.1 equiv) in DMF. Vigorous gas evolution was observed. Once gas evolution had ceased, **m1** (1 equiv) was added dropwise neatly. The reaction mixture was allowed to stir at room temperature for 3–5 h and then partitioned between ethyl acetate and 0.5 M HCl solution. The layers were separated, and the organic layer was washed with water and brine and then concentrated under reduced pressure to provide the crude product. Purification of the crude material by silica gel chromatography (25–55% EtOAc in hexane) afforded **m2**

(yield: 40–77%).

A suspension of **m2** and palladium on carbon (10 wt%) was exposed to an atmosphere of hydrogen (balloon) overnight (~20 h). Analysis of the crude reaction mixture by TLC confirmed the formation of the desired product. The slurry was filtered through diatomite, and the filtrate was concentrated under reduced pressure to give **m3** (yield: 80–98%).

HATU (1 equiv) was added over 2–5 min to a solution of **m3** (1 equiv) and DIPEA (2 equiv) in DMSO. The reaction mixture was stirred at room temperature for 30–50 min. Addition of water resulted in the formation of a precipitate. The mixture was cooled in an ice bath for 15–30 min and then filtered. The collected solid was washed with water and dried in vacuum to afford **m4** (yield: 30–50%).

The iodomethane, iodoethane or iodomethane-d_3 (1.2 equiv) was added dropwise over 15–30 min to a solution of **m4** (1 equiv) and Cs_2CO_3 (1.4 equiv) in DMF stirred under nitrogen at room temperature. The reaction mixture was stirred at room temperature for another 16–20 h. TLC showed that the reaction was completed. The reaction mixture was poured into cold water, which formed a solid. The resultant solid was filtered, and the filter was washed with water and dried in vacuum to afford **m5** (yield: 40–70%).

A one-necked flask, equipped with a magnetic stirrer bar was charged with **m5** (1 equiv), Lawesson's reagent (0.55 equiv) and toluene. The reaction was stirred at 115 °C overnight. Upon completion (monitored by TLC), toluene was removed under vacuum to provide the crude product. Purification of the crude material by silica gel chromatography (10–25% EtOAc in petroleum ether) afforded **m6** (yield: 30–60%).

A solution of **m5** or **m6** (1 equiv) in DCM was treated with HCl (4 N in dioxane, 5 equiv). Evolution of gas was observed, and the reaction mixture was stirred at room temperature for 4–8 h. The resulting solid was filtered off, washed with DCM, and dried to give **m7** or **m8** (yield: 50–90%).

HATU (1 equiv) was added in one portion to a solution of 5-benzyl-4H-1,2,4-triazole-3-carboxylic acid (1.2 equiv) and DIPEA (2 equiv) in DMSO. After 5–10 min of stirring at room temperature, a solution of **m7** or **m8** (1 equiv) in DMSO was added dropwise to the reaction. The reaction mixture was allowed to stir at room temperature for 45–90 min, at which time TLC analysis indicated the reaction was completed. The reaction mixture was extracted with EtOAc. The combined organic solution was washed with brine and concentrated in vacuum to give the crude product. This was purified using silica gel chromatography (eluting with 5–10% MeOH in DCM) to give the target compounds **1**–**26** (yield: 70–90%).

4.2.1. 5-Benzyl-N-(5-methyl-4-oxo-2,3,4,5-tetrahydrobenzo[b][1,4]oxazepin-3-yl)-4H-1,2,4-triazole-3-carboxamide (**1** and **2**)

White solid (23 mg, yield: 80%). m.p.: 109.4–110.8 °C. ^{1}H NMR (300 MHz, DMSO-d_6) δ 14.39 (s, 1H), 8.41 (s, 1H), 7.50 (dd, J = 7.1, 2.3 Hz, 1H), 7.36–7.20 (m, 8H), 4.82 (dt, J = 11.5, 7.8 Hz, 1H), 4.59 (t, J = 10.7 Hz, 1H), 4.40 (dd, J = 9.8, 7.7 Hz, 1H), 4.12 (s, 2H), 3.31 (s, 3H). ^{13}C NMR (75 MHz, DMSO-d_6) δ 168.97, 149.94, 136.91, 129.05, 127.68, 127.16, 126.23, 124.05, 122.95, 76.35, 49.23, 35.29, 32.87. HRMS (ESI, positive) m/z calcd for $C_{20}H_{20}N_5O_3$ $[M+H]^+$ 378.1566; found 378.1573. HPLC analysis: retention time = 7.40 (**1**), 7.50 (**2**) min; peak area, >95%.

4.2.2. 5-Benzyl-N-(1-methyl-2-oxo-1,2,3,4-tetrahydropyrido[2,3-b][1,4]oxazepin-3-yl)-4H-1,2,4-triazole-3-carboxamide (**3** and **4**)

White solid (15 mg, yield: 70%). m.p.: 119.1–120.7 °C. ^{1}H NMR (300 MHz, DMSO-d_6) δ 14.47 (s, 1H), 8.12 (dd, J = 7.5, 1.5 Hz, 1H), 7.84 (dd, J = 4.8, 1.5 Hz, 1H), 7.30 (m, 6H), 7.01 (dd, J = 7.5, 5.1 Hz, 1H), 5.53–5.33 (m, 1H), 4.47–4.23 (m, 2H), 4.13 (s, 2H), 3.05 (s, 3H). ^{13}C NMR (150 MHz, DMSO-d_6) δ 170.42, 158.49, 149.49, 146.56, 145.49, 138.88, 137.57, 132.28, 129.06, 129.00, 127.09, 125.77, 124.75, 79.07, 54.09, 35.81. HRMS (ESI, positive) m/z calcd for $C_{19}H_{19}N_6O_3$ $[M+H]^+$ 379.1519; found 379.1539. HPLC analysis: retention time = 7.57 (**3**), 7.63 (**4**) min; peak area, >95%.

4.2.3. 5-Benzyl-N-(1,7-dimethyl-2-oxo-1,2,3,4-tetrahydropyrido[2,3-b][1,4]oxazepin-3-yl)-4H-1,2,4-triazole-3-carboxamide (**5** and **6**)

White solid (30 mg, yield: 82%). m.p.: 96.0–97.9 °C. ^{1}H NMR (300 MHz, DMSO-d_6) δ 8.50 (d, J = 7.2 Hz, 1H), 7.86 (d, J = 8.1 Hz, 1H), 7.30 (m, 6H), 4.86 (dt, J = 15.3, 7.5 Hz, 1H), 4.66 (t, J = 10.2 Hz, 1H), 4.51 (dd, J = 9.6, 7.5 Hz, 1H), 4.12 (s, 2H), 3.28 (s, 3H), 2.44 (s, 3H). ^{13}C NMR (151 MHz, DMSO-d_6) δ 168.71, 155.25, 154.92, 133.70, 129.05, 128.64, 127.16, 121.86, 75.31, 49.13, 40.55, 35.09, 23.62. HRMS (ESI, positive) m/z calcd for $C_{20}H_{21}N_6O_3$ $[M+H]^+$ 393.1675; found 393.1679. HPLC analysis: retention time = 6.92 (**5**), 6.97 (**6**) min; peak area, >95%.

4.2.4. 5-Benzyl-N-(1,8-dimethyl-2-oxo-1,2,3,4-tetrahydropyrido[2,3-b][1,4]oxazepin-3-yl)-4H-1,2,4-triazole-3-carboxamide (**7** and **8**)

White solid (28 mg, yield: 76%). m.p.: 121.3–122.5 °C. ^{1}H NMR (600 MHz, DMSO-d_6) δ 8.53 (s, 1H), 8.03 (s, 1H), 7.84 (s, 1H), 7.36–7.23 (m, 5H), 4.87 (dt, J = 16.8, 7.8 Hz, 1H), 4.66 (t, J = 9.6 Hz, 1H), 4.56–4.47 (m, 1H), 4.13 (s, 2H), 3.31 (s, 3H), 2.34 (s, 3H). ^{13}C NMR (150 MHz, DMSO-d_6) δ 168.81, 154.18, 145.41, 133.72, 132.31, 131.00, 129.05, 127.17, 75.27, 55.35, 49.24, 35.02, 17.59. HRMS (ESI, positive) m/z calcd for $C_{20}H_{21}N_6O_3$ $[M+H]^+$ 393.1675; found 393.1691. HPLC analysis: retention time = 8.07 (**7**), 8.10 (**8**) min; peak area, >95%.

4.2.5. 5-Benzyl-N-(5-methyl-4-oxo-2,3,4,5-tetrahydropyrido[3,2-b][1,4]oxazepin-3-yl)-4H-1,2,4-triazole-3-carboxamide (**9** and **10**)

White solid (19 mg, yield: 75%). m.p.: 75.7–77.3 °C. ^{1}H NMR (300 MHz, DMSO-d_6) δ 14.36 (s, 1H), 8.53 (d, J = 6.0 Hz, 1H), 8.36 (dd, J = 4.8, 1.5 Hz, 1H), 7.76–7.62 (m, 1H), 7.39–7.13 (m, 6H), 4.91–4.63 (m, 2H), 4.56–4.45 (m, 1H), 4.14 (s, 2H), 3.35 (s, 3H). ^{13}C NMR (150 MHz, DMSO-d_6) δ 169.36, 149.56, 145.52, 144.96, 136.18, 130.11, 129.47, 129.05, 128.67, 127.21, 127.16, 126.94, 76.24, 49.66, 40.89, 33.08. HRMS (ESI, positive) m/z calcd for $C_{19}H_{19}N_6O_3$ $[M+H]^+$ 379.1519; found 379.1517. HPLC analysis: retention time = 7.23 (**9**), 7.29 (**10**) min; peak area, >95%.

4.2.6. 5-Benzyl-N-(5-methyl-4-thioxo-2,3,4,5-tetrahydrobenzo[b][1,4]oxazepin-3-yl)-4H-1,2,4-triazole-3-carboxamide (**11** and **12**)

White solid (21 mg, yield: 75%). m.p.: 124.9–127 °C. ^{1}H NMR (600 MHz, DMSO-d_6) δ 14.36 (s, 1H), 8.53 (d, J = 8.4 Hz, 1H), 7.62 (dd, J = 7.2, 1.8 Hz, 1H), 7.42 (m, 2H), 7.37–7.24 (m, 6H), 5.00 (q, J = 9.0 Hz, 1H), 4.43 (d, J = 8.4 Hz, 2H), 4.16 (s, 2H), 3.80 (s, 3H). ^{13}C NMR (150 MHz, DMSO-d_6) δ 199.57, 158.42, 156.88, 156.52, 149.89, 137.88, 136.91, 129.64, 129.11, 129.05, 128.87, 127.30, 126.81, 126.57, 124.71, 122.95, 79.07, 53.66, 44.76, 32.24. HRMS (ESI, positive) m/z calcd for $C_{20}H_{20}N_5O_2S$ $[M+H]^+$ 394.1338; found 394.1316. HPLC analysis: retention time = 8.19 (**11**), 8.14 (**12**) min; peak area, >95%.

4.2.7. 5-Benzyl-N-(4-thioxo-2,3,4,5-tetrahydrobenzo[b][1,4]oxazepin-3-yl)-4H-1,2,4-triazole-3-carboxamide (**13** and **14**)

White solid (15 mg, yield: 77%). m.p.: 124.7–126.5 °C. ^{1}H NMR (300 MHz, DMSO-d_6) δ 14.32 (s, 1H), 10.11 (s, 1H), 8.37 (s, 1H), 7.33–7.04 (m, 9H), 4.75 (dt, J = 14.7, 7.5 Hz, 1H), 4.54–4.32 (m, 2H), 4.08 (s, 2H). ^{13}C NMR (150 MHz, DMSO-d_6) δ 200.92, 170.81, 149.96, 136.90, 131.89, 129.06, 128.30, 127.23, 125.35, 123.75, 122.75, 78.33, 60.22, 29.45. HRMS (ESI, positive) m/z calcd for $C_{19}H_{18}N_5O_2S$ $[M+H]^+$ 380.1181; found 380.1184. HPLC analysis: retention

time = 7.38 (**13**), 7.40 (**14**) min; peak area, >95%.

4.2.8. 5-Benzyl-N-(5-(methyl-d_3)-4-thioxo-2,3,4,5-tetrahydrobenzo[b][1,4]oxazepin-3-yl)-4H-1,2,4-triazole-3-carboxamide (*15* and *16*)

White solid (40 mg, yield: 81%). m.p.: 93.3–95.5 °C. ^{1}H NMR (600 MHz, DMSO-d_6) δ 14.36 (s, 1H), 8.53 (s, 1H), 7.62 (d, J = 6.6 Hz, 1H), 7.47–7.22 (m,8H), 4.99 (dd, J = 16.2, 7.8 Hz, 1H), 4.43 (d, J = 7.8 Hz, 2H), 4.16 (s, 2H). ^{13}C NMR (150 MHz, DMSO-d_6) δ 199.59, 158.40, 156.88, 156.52, 149.89, 137.85, 136.93, 129.63, 129.06, 127.29, 126.57, 124.69, 122.95, 79.05, 53.68, 38.71, 32.24. HRMS (ESI, positive) m/z calcd for $C_{20}H_{17}D_3N_5O_2S$ $[M+H]^+$ 397.1526; found 397.1522. HPLC analysis: retention time = 8.12 (**15**), 8.08 (**16**) min; peak area, >95%.

4.2.9. 5-Benzyl-N-(5-ethyl-4-thioxo-2,3,4,5-tetrahydrobenzo[b][1,4]oxazepin-3-yl)-4H-1,2,4-triazole-3-carboxamide (*17* and *18*)

White solid (21 mg, yield: 75%). m.p.: 156.3–158.1 °C. ^{1}H NMR (600 MHz, DMSO-d_6) δ 8.59 (d, J = 7.2 Hz, 1H), 7.68 (dd, J = 7.8, 1.2 Hz, 1H), 7.47–7.40 (m, 2H), 7.36–7.23 (m, 6H), 4.97 (dt, J = 15.6, 7.8 Hz, 1H), 4.82 (m, 1H), 4.43 (m, 1H), 4.39 (m, 1H), 4.14 (s, 2H), 4.09 (m, 1H), 1.14 (t, J = 6.6 Hz, 3H). ^{13}C NMR (150 MHz, DMSO-d_6) δ 199.24, 157.89, 150.71, 137.37, 136.06, 129.92, 129.06, 127.16, 126.72, 124.77, 122.98, 79.19, 53.65, 50.83, 32.72, 11.63. HRMS (ESI, positive) m/z calcd for $C_{21}H_{22}N_5O_2S$ $[M+H]^+$ 408.1494; found 408.1493. HPLC analysis: retention time = 8.57 (**17**), 8.61 (**18**) min; peak area, >95%.

4.2.10. 5-benzyl-N-(1-methyl-2-thioxo-1,2,3,4-tetrahydropyrido[2,3-b][1,4]oxazepin-3-yl)-4H-1,2,4-triazole-3-carboxamide (*19* and *20*)

White solid (18 mg, yield: 74%). m.p.: 113.2–114.9. ^{1}H NMR (600 MHz, DMSO-d_6) δ 8.55 (s, 1H), 8.08 (dd, J = 7.6, 1.8 Hz, 1H), 7.93 (dd, J = 4.9, 1.8 Hz, 1H), 7.40–7.22 (m, 5H), 7.08 (dd, J = 7.7, 4.9 Hz, 1H), 5.72 (m, 1H), 4.64 (dd, J = 10.5, 4.4 Hz, 1H), 4.30 (t, J = 10.4 Hz, 1H), 4.15 (s, 2H), 3.50 (s, 3H). ^{13}C NMR (150 MHz, DMSO-d_6) δ 204.22, 157.63, 156.88, 147.37, 138.31, 137.75, 129.05, 129.02, 127.50, 127.14, 118.31, 69.54, 52.54, 44.58. HRMS (ESI, positive) m/z calcd for $C_{19}H_{19}N_6O_2S$ $[M+H]^+$ 395.1290; found 395.1291. HPLC analysis: retention time = 7.22 (**19**), 7.22 (**20**) min; peak area, >95%.

4.2.11. 5-Benzyl-N-(1,7-dimethyl-2-thioxo-1,2,3,4-tetrahydropyrido[2,3-b][1,4]oxazepin-3-yl)-4H-1,2,4-triazole-3-carboxamide (*21* and *22*)

White solid (16 mg, yield: 71%). m.p.: 114.5–116.1 °C. ^{1}H NMR (300 MHz, DMSO-d_6) δ 14.36 (s, 1H), 8.56 (d, J = 7.8 Hz, 1H), 7.98 (d, J = 8.1 Hz, 1H), 7.41–7.18 (m, 6H), 5.14–4.92 (m, 1H), 4.52 (d, J = 8.7 Hz, 2H), 4.15 (s, 2H), 3.76 (s, 3H), 2.48 (s, 3H). ^{13}C NMR (75 MHz, DMSO-d_6) δ 202.92, 161.35, 160.50, 158.49, 144.76, 140.73, 138.00, 133.16, 132.48, 130.60, 125.74, 81.49, 57.04, 36.09, 27.24, 22.27. HRMS (ESI, positive) m/z calcd for $C_{20}H_{21}N_6O_2S$ $[M+H]^+$ 409.1447; found 409.1449. HPLC analysis: retention time = 7.48 (**21**), 7.48 (**22**) min; peak area, >95%.

4.2.12. 5-Benzyl-N-(1,8-dimethyl-2-thioxo-1,2,3,4-tetrahydropyrido[2,3-b][1,4]oxazepin-3-yl)-4H-1,2,4-triazole-3-carboxamide (*23* and *24*)

White solid (28 mg, yield: 84%). m.p.: 116.1–117.1 °C. ^{1}H NMR (600 MHz, DMSO-d_6) δ 8.58 (d, J = 6.0 Hz, 1H), 8.16 (dd, J = 1.8, 0.6 Hz, 1H), 7.98 (d, J = 1.8 Hz, 1H), 7.37–7.22 (m, 6H), 5.01 (q, J = 9.0 Hz, 1H), 4.52 (d, J = 7.8 Hz, 2H), 4.16 (s, 2H), 3.78 (s, 3H), 2.38 (s, 3H). ^{13}C NMR (150 MHz, DMSO-d_6) δ 199.88, 156.93, 153.99, 147.34, 136.87, 134.69, 132.90, 131.93, 129.11, 129.04, 127.32, 78.08, 53.66, 44.52, 32.22, 17.59. HRMS (ESI, positive) m/z calcd for $C_{20}H_{21}N_6O_2S$ $[M+H]^+$ 409.1447; found 409.1448. HPLC analysis: retention time = 8.02 (**23**), 8.02 (**24**) min; peak area, >95%.

4.2.13. 5-Benzyl-N-(5-methyl-4-thioxo-2,3,4,5-tetrahydropyrido[3,2-b][1,4]oxazepin-3-yl)-4H-1,2,4-triazole-3-carboxamide (*25* and *26*)

White solid (28 mg, yield: 76%). m.p.: 115.0–117.1 °C. ^{1}H NMR (600 MHz, DMSO-d_6) δ 8.72 (s, 1H), 8.47 (dd, J = 4.8, 1.8 Hz, 1H), 7.80 (dd, J = 7.8, 1.2 Hz, 1H), 7.49 (dd, J = 7.8, 4.8 Hz, 1H), 7.40–7.21 (m, 6H), 5.02 (dt, J = 14.4, 7.2 Hz, 1H), 4.63 (t, J = 10.2 Hz, 1H), 4.53 (dd, J = 10.2, 7.2 Hz, 1H), 4.14 (s, 2H), 3.81 (s, 3H). ^{13}C NMR (150 MHz, DMSO-d_6) δ 195.52, 157.45, 149.49, 146.23, 145.50, 140.66, 140.46, 139.94, 129.05, 129.01, 127.14, 124.09, 121.93, 89.63, 79.04, 40.93, 35.64. HRMS (ESI, positive) m/z calcd for $C_{19}H_{19}N_6O_2S$ $[M+H]^+$ 395.1290; found 395.1289. HPLC analysis: retention time = 9.28 (**25**), 9.28 (**26**) min; peak area, >95%.

4.2. Molecular modeling

Chemical structures for each of the compounds were generated with the lowest energy ring conformations using Schrodinger LigPrep package by default parameters following our previous protocols [24,25].

4.3. Biology

4.3.1. Reagents

Dulbecco's modified Eagle's medium (DMEM), fetal bovine serum (FBS), penicillin–streptomycin liquid (100×), phosphate buffer saline (PBS). The 2,3,5-triphenyl tetrazolium chloride (TTC) was obtained from BIO BASICINC (Shanghai, China). Recombinant mouse/human TNF-α were purchased from Novoprotein (Shanghai, China). Z-VAD-fmk (T6013) was purchased from Targetmol (Targetmol, USA). Smac mimetic (HY-15989) were purchased from MedChemExpress (Monmouth Junction, NJ, USA).

4.4. Cell culture and transfection

HT-29 (NCI-DTP Cat# HT-29) cells were cultured in DMEM with 10% FBS (v/v), 1% L-glutamine and 100 U/mL penicillin/streptomycin (v/v). Cells were grown at 37 °C in a humidified atmosphere with 5% CO_2 and were harvested in all experiments from exponentially growing cultures.

4.5. Necroptosis induction and cell viability assays

Necroptosis was induced by pre-treatment with z-VAD-fmk (20 μM) and Smac mimetic (10 nM) for 30 min and followed by TNF-α (20 ng/mL) for 8–10 h. Apoptosis was induced by TNF-α (40 ng/mL) and Smac mimetic (20 nM) for 30 h. The compounds were incubated with the cells exposed to one of the above combinations at the indicated concentrations for 8–10 h or 30 h. Cell viability was then examined by using the CellTiter-Glo Luminescent Cell Viability Assay kit. Luminescence was recorded with a SpectraMax M5e microplate reader.

4.6. Western blotting

After compound treatment, the protein samples were extracted from cells using RIPA lysis buffer containing a protease inhibitor and phosphatase inhibitor cocktail (Beyotime Biotechnology, China), The quantification of proteins was analyzed using BCA protein assay kit (Beyotime Biotechnology, China). The proteins (30 μg) were resolved over sodium dodecyl sulfate-polyacrylamide gel electrophoresis (SDS-PAGE) and transferred to PVDF membranes (Millipore, Bedford, MA, U.S.A.). Then, the membranes were

blocked in 5% BSA for 2 h. Primary antibodies were prepared in 1% BSA at a dilution of 1:1000. The blocked membranes were incubated with corresponding antibody overnight at 4 °C, followed by the incubation with marked secondary antibody (1:8000) for 1 h at room temperature. The signals were captured and analyzed using the LI-COR Odyssey system. Antibodies were from commercial sources: anti-human-RIPK1 (Abcam Cat# 3493s); anti-human phospho-RIPK1 (Cell Signaling Technology, Cat# 65746S); anti-human-RIPK3 (Abcam Cat# ab56164), anti-human phospho-RIPK3 (Abcam Cat# ab209384), anti-human MLKL (Abcam Cat# ab184718), anti-human phospho-MLKL (Abcam Cat# 187091), anti-GAPDH (Abcam Cat# ab181602).

4.7. Immunoprecipitation

Cells were lysed with Nonidet P-40 buffer (Beyotime Biotechnology, China) supplemented with 1 mM PMSF, 1 × protease inhibitor mixture (Roche), 10 mM β-glycerophosphate, 5 mM NaF, and 1 mM Na_3VO_4. The lysates were centrifuged and the supernatants were incubated with anti-RIPK1 (CST Cat# 3493S) antibody overnight at 4 °C. The immunocomplex was captured by Protein A/G Agarose (Life Technologies) overnight at 4 °C. Beads were washed three times with PBS, and the bound proteins were removed by boiling in SDS buffer, and the samples were resolved in 10% SDS-polyacrylamide gels by western blotting analysis.

4.8. Statistical analysis

The one-way analysis of variance was used to compare differences among groups represented by the mean values ± SD. $P < 0.05$ was considered statistically significant.

Declaration of competing interest

The authors declare that they have no known competing financial interests or personal relationships that could have appeared to influence the work reported in this paper.

Acknowledgments

This work was funded by grants from the National Natural Science Foundation of China (82022065, 81872791, 82073696, and U20A20136).

Appendix A. Supplementary data

Supplementary data to this article can be found online at https://doi.org/10.1016/j.ejmech.2021.113484.

References

[1] T. Vanden Berghe, A. Linkermann, S. Jouan-Lanhouet, H. Walczak, P. Vandenabeele, Regulated necrosis: the expanding network of non-apoptotic cell death pathways, Nat. Rev. Mol. Cell Biol. 15 (2014) 135–147.
[2] P. Vandenabeele, L. Galluzzi, T. Vanden Berghe, G. Kroemer, Molecular mechanisms of necroptosis: an ordered cellular explosion, Nat. Rev. Mol. Cell Biol. 11 (2010) 700–714.
[3] M. Pasparakis, P. Vandenabeele, Necroptosis and its role in inflammation, Nature 517 (2015) 311–320.
[4] L. Mifflin, D. Ofengeim, J. Yuan, Receptor-interacting protein kinase 1 (RIPK1) as a therapeutic target, Nat. Rev. Drug Discov. 19 (2020) 553–571.
[5] S. Grootjans, T. Vanden Berghe, P. Vandenabeele, Initiation and execution mechanisms of necroptosis: an overview, Cell Death Differ. 24 (2017) 1184–1195.
[6] A. Degterev, J. Hitomi, M. Germscheid, I.L. Ch'en, O. Korkina, X. Teng, D. Abbott, G.D. Cuny, C. Yuan, G. Wagner, S.M. Hedrick, S.A. Gerber, A. Lugovskoy, J. Yuan, Identification of RIP1 kinase as a specific cellular target of necrostatins, Nat. Chem. Biol. 4 (2008) 313–321.
[7] A. Degterev, Z. Huang, M. Boyce, Y. Li, P. Jagtap, N. Mizushima, G.D. Cuny, T.J. Mitchison, M.A. Moskowitz, J. Yuan, Chemical inhibitor of nonapoptotic cell death with therapeutic potential for ischemic brain injury, Nat. Chem. Biol. 1 (2005) 112–119.
[8] Y.S. Cho, S. Challa, D. Moquin, R. Genga, T.D. Ray, M. Guildford, F.K. Chan, Phosphorylation-driven assembly of the RIP1-RIP3 complex regulates programmed necrosis and virus-induced inflammation, Cell 137 (2009) 1112–1123.
[9] S. He, L. Wang, L. Miao, T. Wang, F. Du, L. Zhao, X. Wang, Receptor interacting protein kinase-3 determines cellular necrotic response to TNF-alpha, Cell 137 (2009) 1100–1111.
[10] Z. Cai, S. Jitkaew, J. Zhao, H.C. Chiang, S. Choksi, J. Liu, Y. Ward, L.G. Wu, Z.G. Liu, Plasma membrane translocation of trimerized MLKL protein is required for TNF-induced necroptosis, Nat. Cell Biol. 16 (2014) 55–65.
[11] J. Zhao, S. Jitkaew, Z. Cai, S. Choksi, Q. Li, J. Luo, Z.G. Liu, Mixed lineage kinase domain-like is a key receptor interacting protein 3 downstream component of TNF-induced necrosis, Proc. Natl. Acad. Sci. U. S. A. 109 (2012) 5322–5327.
[12] X. Chen, W. Li, J. Ren, D. Huang, W.T. He, Y. Song, C. Yang, W. Li, X. Zheng, P. Chen, J. Han, Translocation of mixed lineage kinase domain-like protein to plasma membrane leads to necrotic cell death, Cell Res. 24 (2014) 105–121.
[13] Y. Dondelinger, W. Declercq, S. Montessuit, R. Roelandt, A. Goncalves, I. Bruggeman, P. Hulpiau, K. Weber, C.A. Sehon, R.W. Marquis, J. Bertin, P.J. Gough, S. Savvides, J.C. Martinou, M.J. Bertrand, P. Vandenabeele, MLKL compromises plasma membrane integrity by binding to phosphatidylinositol phosphates, Cell Rep. 7 (2014) 971–981.
[14] H. Wang, L. Sun, L. Su, J. Rizo, L. Liu, L.F. Wang, F.S. Wang, X. Wang, Mixed lineage kinase domain-like protein MLKL causes necrotic membrane disruption upon phosphorylation by RIP3, Mol. Cell 54 (2014) 133–146.
[15] C. Zhuang, F. Chen, Small-Molecule inhibitors of necroptosis: current status and perspectives, J. Med. Chem. 63 (2020) 1490–1510.
[16] P.A. Harris, B.W. King, D. Bandyopadhyay, S.B. Berger, N. Campobasso, C.A. Capriotti, J.A. Cox, L. Dare, X. Dong, J.N. Finger, L.C. Grady, S.J. Hoffman, J.U. Jeong, J. Kang, V. Kasparcova, A.S. Lakdawala, R. Lehr, D.E. McNulty, R. Nagilla, M.T. Ouellette, C.S. Pao, A.R. Rendina, M.C. Schaeffer, J.D. Summerfield, B.A. Swift, R.D. Totoritis, P. Ward, A. Zhang, D. Zhang, R.W. Marquis, J. Bertin, P.J. Gough, DNA-encoded library screening identifies benzo[b][1,4]oxazepin-4-ones as highly potent and monoselective receptor interacting protein 1 kinase inhibitors, J. Med. Chem. 59 (2016) 2163–2178.
[17] M. Yoshikawa, M. Saitoh, T. Katoh, T. Seki, S.V. Bigi, Y. Shimizu, T. Ishii, T. Okai, M. Kuno, H. Hattori, E. Watanabe, K.S. Saikatendu, H. Zou, M. Nakakariya, T. Tatamiya, Y. Nakada, T. Yogo, Discovery of 7-oxo-2,4,5,7-tetrahydro-6 h-pyrazolo[3,4- c]pyridine derivatives as potent, orally available, and brain-penetrating receptor interacting protein 1 (RIP1) kinase inhibitors: analysis of structure-kinetic relationships, J. Med. Chem. 61 (2018) 2384–2409.
[18] P.A. Harris, S.B. Berger, J.U. Jeong, R. Nagilla, D. Bandyopadhyay, N. Campobasso, C.A. Capriotti, J.A. Cox, L. Dare, X. Dong, P.M. Eidam, J.N. Finger, S.J. Hoffman, J. Kang, V. Kasparcova, B.W. King, R. Lehr, Y. Lan, L.K. Leister, J.D. Lich, T.T. MacDonald, N.A. Miller, M.T. Ouellette, C.S. Pao, A. Rahman, M.A. Reilly, A.R. Rendina, E.J. Rivera, M.C. Schaeffer, C.A. Sehon, R.R. Singhaus, H.H. Sun, B.A. Swift, R.D. Totoritis, A. Vossenkamper, P. Ward, D.D. Wisnoski, D. Zhang, R.W. Marquis, P.J. Gough, J. Bertin, Discovery of a first-in-class receptor interacting protein 1 (RIP1) kinase specific clinical candidate (GSK2982772) for the treatment of inflammatory diseases, J. Med. Chem. 60 (2017) 1247–1261.
[19] K. Weisel, N.E. Scott, D.J. Tompson, B.J. Votta, S. Madhavan, K. Povey, A. Wolstenholme, M. Simeoni, T. Rudo, L. Richards-Peterson, T. Sahota, J.G. Wang, J. Lich, J. Finger, A. Verticelli, M. Reilly, P.J. Gough, P.A. Harris, J. Bertin, M.L. Wang, Randomized clinical study of safety, pharmacokinetics, and pharmacodynamics of RIPK1 inhibitor GSK2982772 in healthy volunteers, Pharmacol. Res. Perspect. 5 (2017), e00365.
[20] P.A. Harris, J.M. Marinis, J.D. Lich, S.B. Berger, A. Chirala, J.A. Cox, P.M. Eidam, J.N. Finger, P.J. Gough, J.U. Jeong, J. Kang, V. Kasparcova, L.K. Leister, M.K. Mahajan, G. Miller, R. Nagilla, M.T. Ouellette, M.A. Reilly, A.R. Rendina, E.J. Rivera, H.H. Sun, J.H. Thorpe, R.D. Totoritis, W. Wang, D. Wu, D. Zhang, J. Bertin, R.W. Marquis, Identification of a RIP1 kinase inhibitor clinical candidate (GSK3145095) for the treatment of pancreatic cancer, ACS Med. Chem. Lett. 10 (2019) 857–862.
[21] C. Zhuang, Z. Miao, L. Zhu, Y. Zhang, Z. Guo, J. Yao, G. Dong, S. Wang, Y. Liu, H. Chen, C. Sheng, W. Zhang, Synthesis and biological evaluation of thio-benzodiazepines as novel small molecule inhibitors of the p53-MDM2 protein-protein interaction, Eur. J. Med. Chem. 46 (2011) 5654–5661.
[22] Z. Guo, C. Zhuang, L. Zhu, Y. Zhang, J. Yao, G. Dong, S. Wang, Y. Liu, H. Chen, C. Sheng, Z. Miao, W. Zhang, Structure-activity relationship and antitumor activity of thio-benzodiazepines as p53-MDM2 protein-protein interaction inhibitors, Eur. J. Med. Chem. 56 (2012) 10–16.
[23] J.U. Jeong, J. Kang, L.K. Leister, J.J. Romano, Process and Intermediates for Preparing Benzoxazepines, 2018, WO2018007973.
[24] C. Zhuang, S. Narayanapillai, W. Zhang, Y.Y. Sham, C. Xing, Rapid identification of Keap1-Nrf2 small-molecule inhibitors through structure-based virtual screening and hit-based substructure search, J. Med. Chem. 57 (2014) 1121–1126.
[25] S. Han, Y. Lei, C. Pannecouque, E. De Clercq, C. Zhuang, F. Chen, Fragment-based discovery of sulfur-containing diarylbenzopyrimidines as novel non-nucleoside reverse transcriptase inhibitors, Chin. Chem. Lett. 31 (2020) 764–768.